Electronic Supplementary Information

Spirobifluorene-based water-soluble imidazolium polymer for luminescent sensing

Caifeng Wei, Jinyi Wu, Xiying Feng, Zujin Yang,*, Jianyong Zhang,* Hongbing Ji*

Sun Yat-Sen University, School of Chemical Engineering and Technology, MOE Laboratory of Polymeric Composite and Functional Materials, School of Materials Science and Engineering, Guangzhou 510275, China.

Materials and methods

^{1}H NMR was measured on a Bruker AVANCE III 400 spectrometer at ambient temperature. ^{13}C NMR was measured on a Bruker Avance III 500HD spectrometer at ambient temperature. Solid-state ^{13}C CP/MAS NMR spectrum was measured on a Bruker AVANCE 400 spectrometer. Fourier transform infrared spectroscopy (FT-IR) was recorded on KBr pellets by a NICOLET 6700 FT-IR instrument in the region 4000-400 cm^{-1}. Scanning electron microscopy (SEM) was performed on SU8010 operated at an accelerating voltage of 5.0 kV. X-ray diffraction (XRD) patterns were collected on the D-MAX 2200 VPC using Cu radiation source at 40 kV and 26 mA, from 5 to 80 °C with a scan rate of 8.0 °C s^{-1}. Thermogravimetric analysis (TGA) was carried out with a TG-209/Vector-22 instrument in nitrogen atmosphere at a heating rate of 10 °C min^{-1}. Liquid UV-Vis spectroscopic analyses were performed on a RIGOL Ultra-3660 spectrophotometer. Dynamic light scattering (DLS) was measured on an EliteSizer Brookhaven instruments at ambient temperature in the solvent of H_2O. N_2 adsorption isotherms were measured at 77 K using an automated Micromeritics ASAP 2460 surface area and porosimetry system, and the sample was degassed at 100°C for 10 h in vacuum before analysis. The surface area was calculated using the Brunauer-Emmett-Teller (BET) method and the pore size distribution was determined by NLDFT method. The fluorescence excitation and emission spectra were performed on a FLSP920 instrument at room temperature. The electrochemical measurement was performed at room temperature using a typical three-electrode cell controlled by a CHI 660E electrochemical workstation.

Quantum yield of IMSPF-Br-COOH in solution was calculated according to the following equation:

$$\varphi = \frac{n^2 A_s D}{n_s^2 A D_s}\varphi_s \quad (\varphi_s = 0.55, A, A_s \leq 0.05)$$

where φ is fluorescence quantum yield, A is the absorbance, n is the refractive index of the solution, and D is the corrected fluorescence emission spectral integral area. Excitation was chosen at 333 nm, $n = n_s$. The subscript "s" refers to the reference fluorophore, quinine sulfate dihydrate dissolved in dilute sulphuric acid (quantum yield, $\varphi_s = 0.55$).

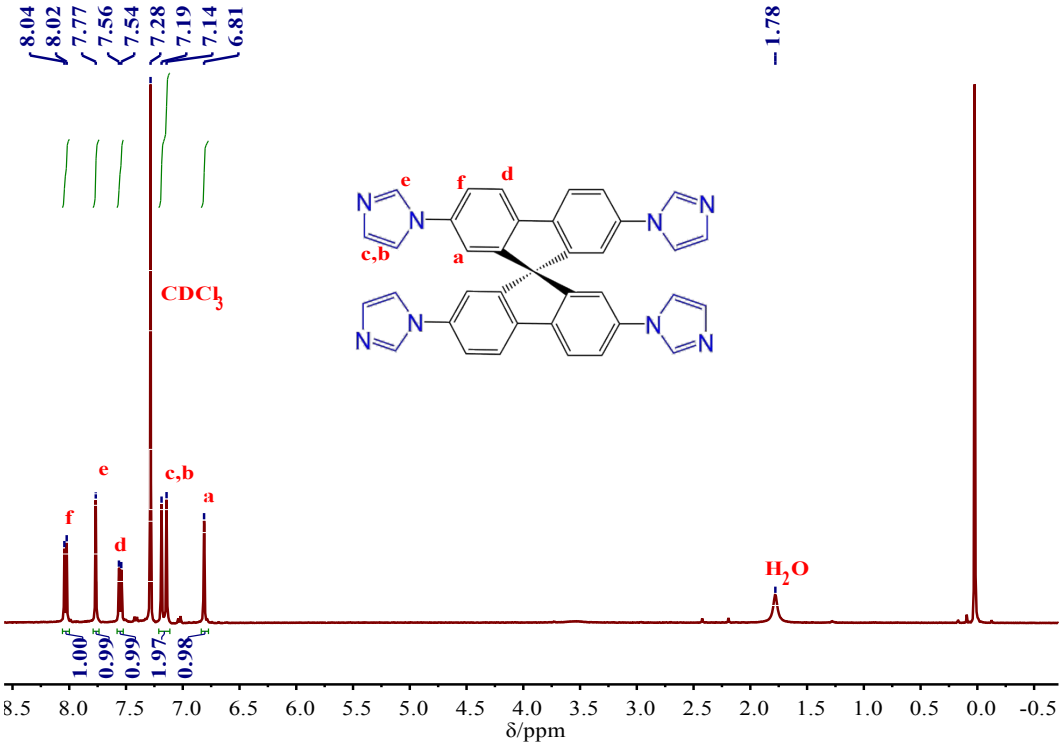

Fig. S1 ^{1}H NMR spectrum of IMSPF (400 MHz, $CDCl_3$).

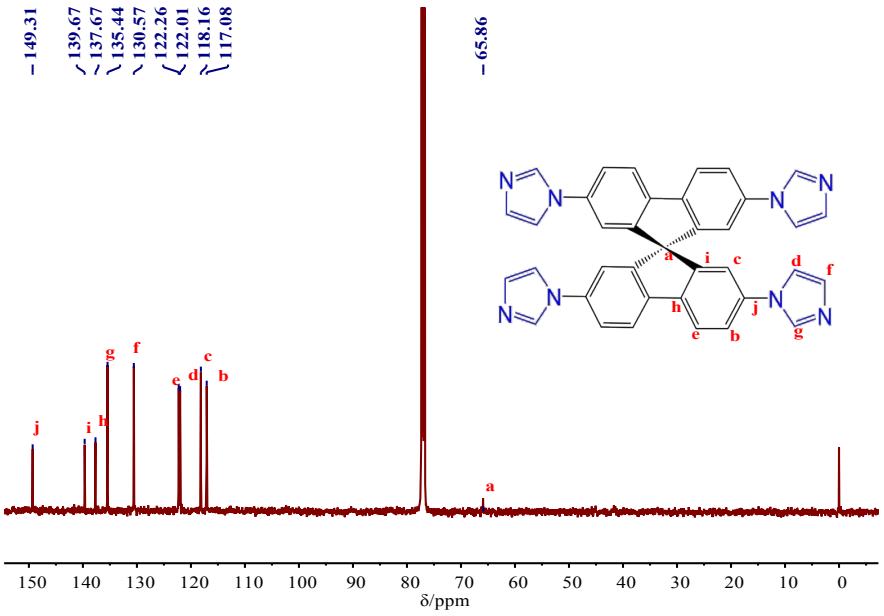

Fig. S2 ^{13}C NMR spectrum of IMSPF (125 MHz, $CDCl_3$).

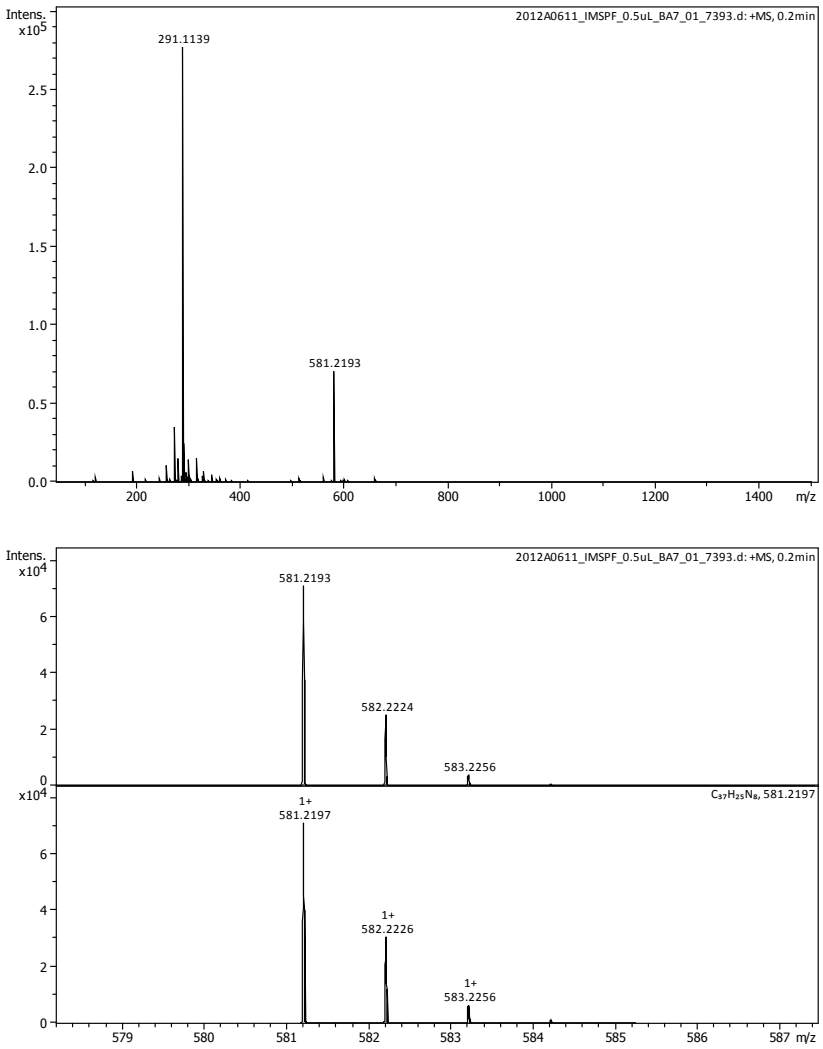

Fig. S3 ESI-TOF-MS spectra of IMSPF: *m/z* found (calcd.) for $[C_{37}H_{25}N_8]^+$, 581.2193 (581.2197).

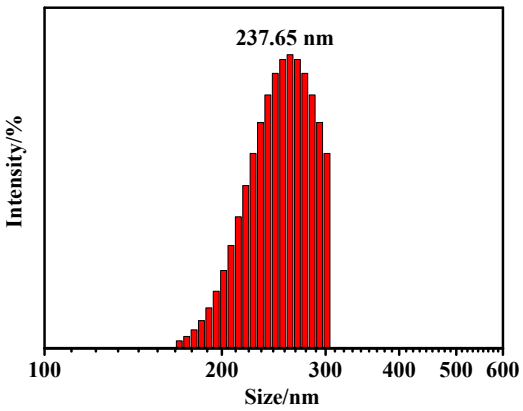

Fig. S4 Dynamic light scattering analysis of the aqueous solution of IMSPF-Br-COOH (0.4 mg mL^{-1}).

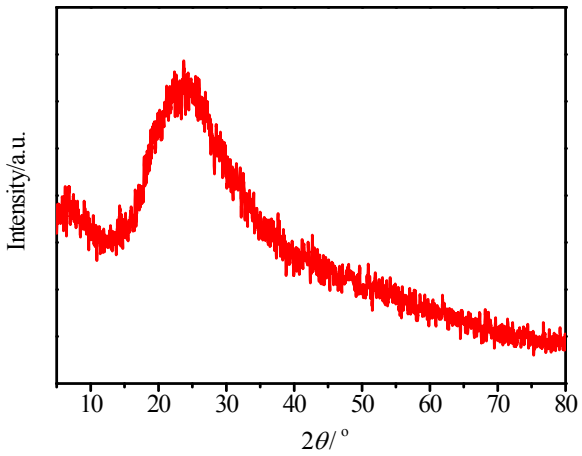

Fig. S5 Powder X-ray diffraction pattern of IMSPF-Br-COOH.

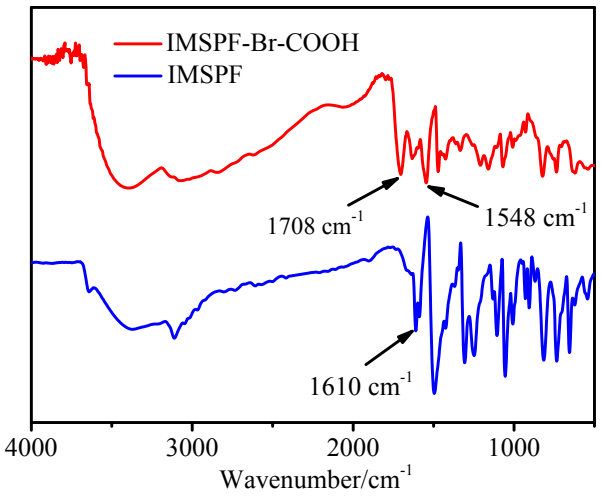

Fig. S6 FT-IR spectra of IMSPF-Br-COOH and IMSPF.

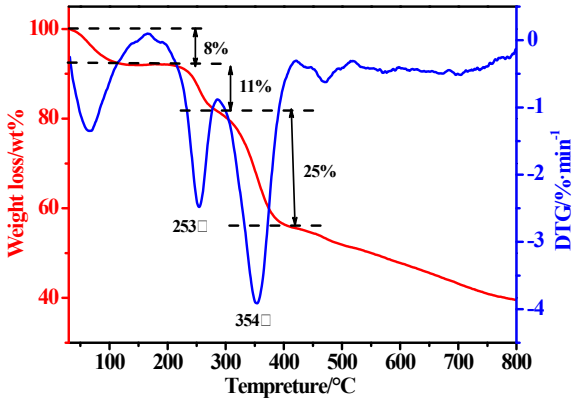

Fig. S7 Thermogravimetric analysis (TGA) curves of IMSPF-Br-COOH under N_2 atmosphere.

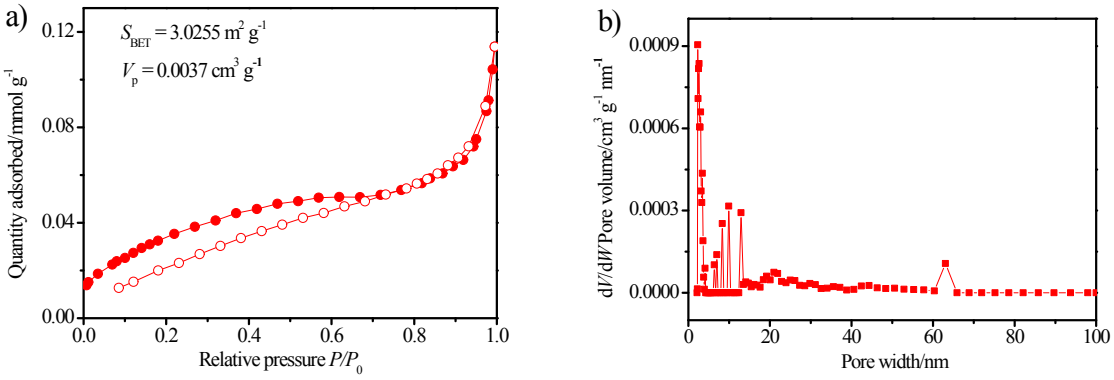

Fig. S8 N_2 adsorption-desorption isotherms and NLDFT pore size distributions of IMSPF-Br-COOH.

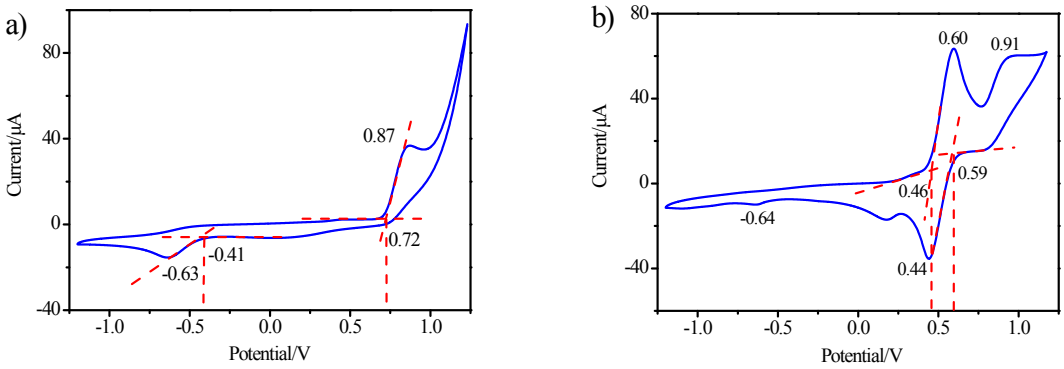

Fig. S9 Cyclic voltammetry of (a) IMSPF-Br-COOH, and (b) IMSPF-Br-COOH using ferrocene as internal reference in 0.1 mol L^{-1} Bu_4NPF_6 in anhydrous DMSO with a scan rate of 0.05 V s^{-1}.

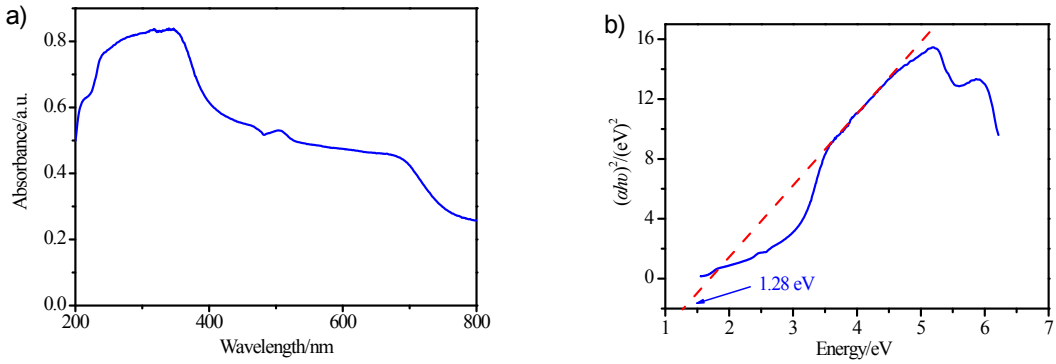

Fig. S10 (a) UV-visible diffuse reflectance spectrum, and (b) Tauc plot of IMSPF-Br-COOH.

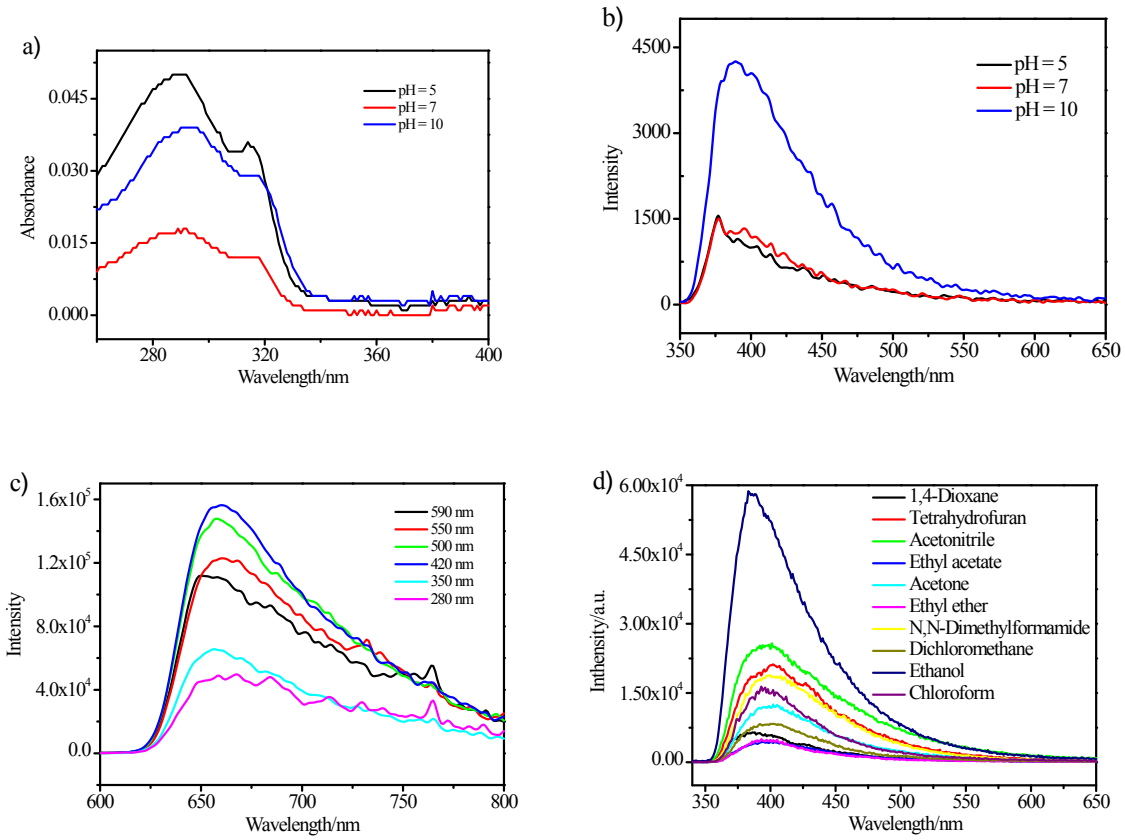

Fig. S11 (a) UV-visible spectra of IMSPF-Br-COOH (7.83×10^{-4} mg mL^{-1}) in water, (b) fluorescence spectra of IMSPF-Br-COOH (7.83×10^{-4} mg mL^{-1}) in water, (c) solid-state fluorescence spectra of IMSPF-Br-COOH with different excitation wavenumbers, (d) fluorescence spectra of IMSPF-Br-COOH in various solvents.

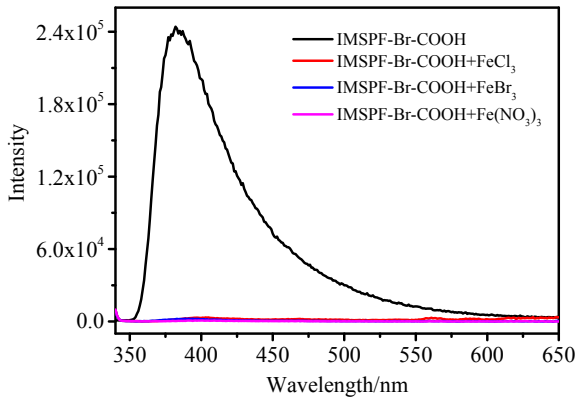

Fig. S12 Emission spectra of the IMSPF-Br-COOH aqueous solution upon addition of $FeCl_3$, $FeBr_3$ and $Fe(NO_3)_3$ (0.40 mg mL^{-1} IMSPF-Br-COOH was dispersed in H_2O containing $FeCl_3$, $FeBr_3$ or $Fe(NO_3)_3$ solutions with a concentration of 1.0×10^{-2} mol L^{-1}).

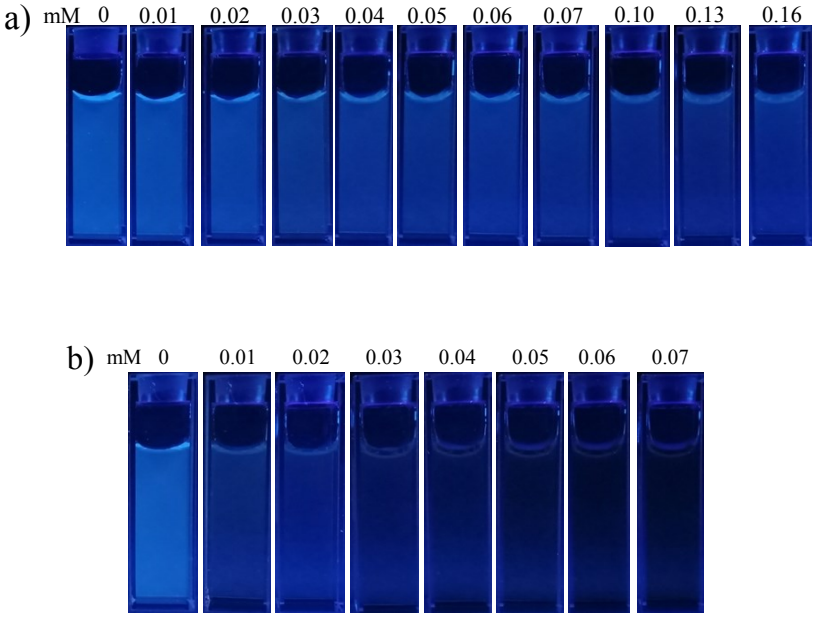

Fig. S13 Fluorescence changes of the IMSPF-Br-COOH aqueous solution with various ion concentrations, (a) Fe^{3+} (from left to right, the concentrations are 0, 0.01, 0.02, 0.03, 0.04, 0.05, 0.06, 0.07, 0.10, 0.13, 0.16 mmol L^{-1}), and (b) $Cr_2O_7^{2-}$ (from left to right, the concentrations are 0, 0.01, 0.02, 0.03, 0.04, 0.05, 0.06, 0.07 mmol L^{-1}).

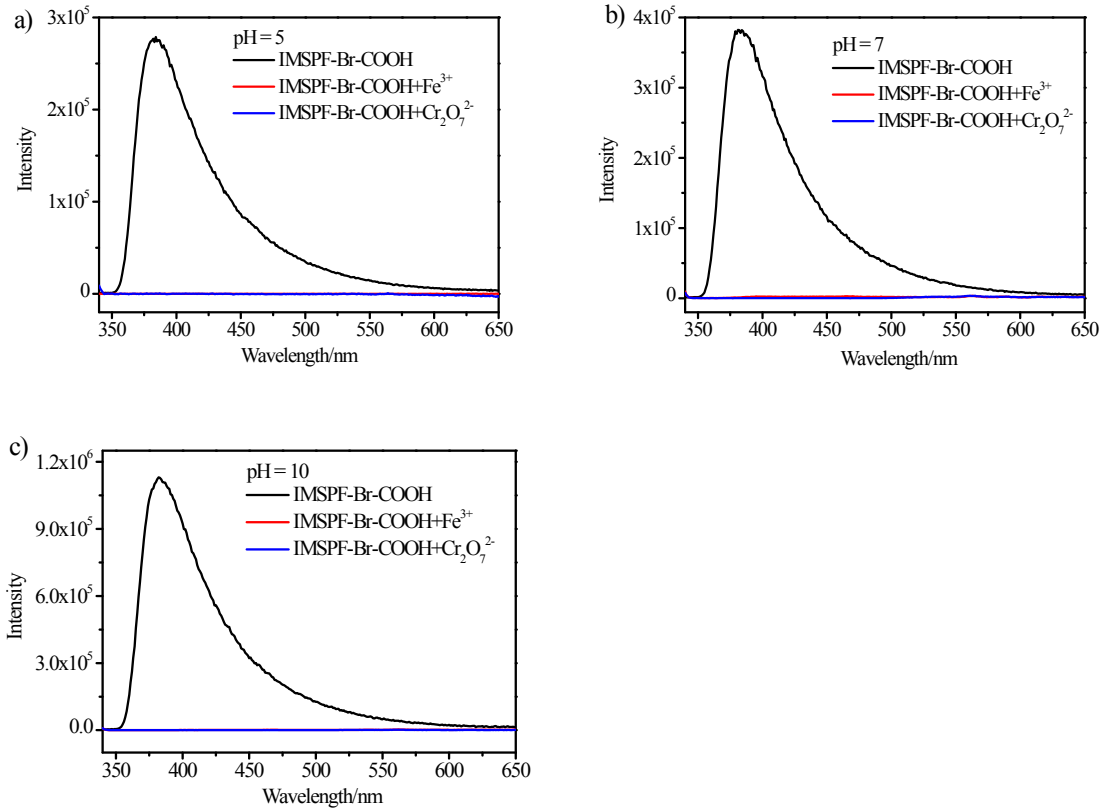

Fig. S14 Emission spectra of the IMSPF-Br-COOH aqueous solution upon addition of Fe^{3+} or $Cr_2O_7^{2-}$ at various pH, a) pH = 5, b) pH = 7, and c) pH = 10 (0.40 mg mL^{-1} of IMSPF-Br-COOH aqueous solution containing $FeCl_3$ or $K_2Cr_2O_7$ solution with a concentration of 1.0×10^{-2} mol L^{-1}).

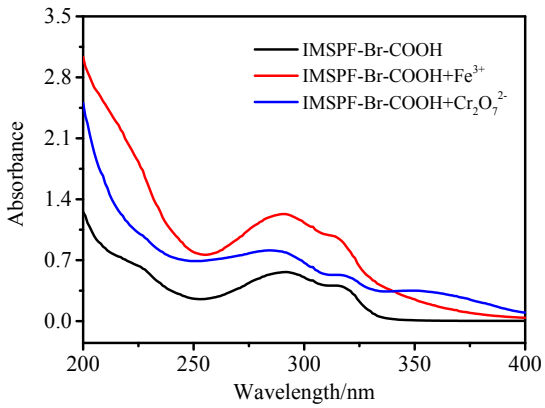

Fig. S15 UV-vis absorption of IMSPF-Br-COOH aqueous solution, IMSPF-Br-COOH+Fe^{3+} and IMSPF-Br-COOH+ $Cr_2O_7^{2-}$ (0.40 mg mL^{-1} of IMSPF-Br-COOH aqueous solution containing $FeCl_3$ or $K_2Cr_2O_7$ solution with a concentration of 1.0×10^{-2} mol L^{-1}).

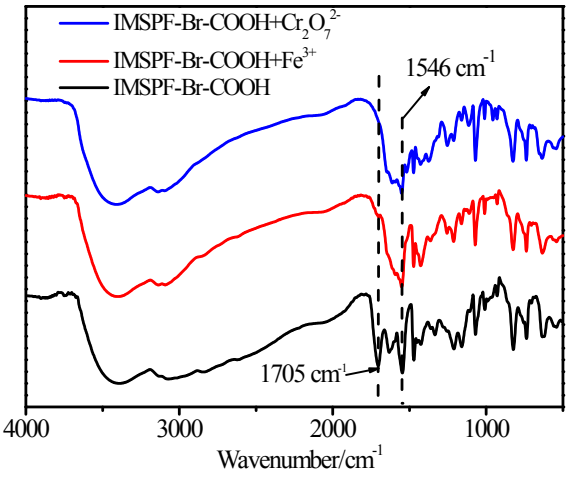

Fig. S16 FT-IR spectra of IMSPF-Br-COOH, IMSPF-Br-COOH+Fe^{3+} and IMSPF-Br-COOH+$Cr_2O_7^{2-}$. (IMSPF-Br-COOH was dispersed in ethanol, and then Fe^{3+} or $Cr_2O_7^{2-}$ was added. The mixture was stirred for 12 h and filtered to obtain IMSPF-Br-COOH+Fe^{3+} or IMSPF-Br-COOH+$Cr_2O_7^{2-}$).

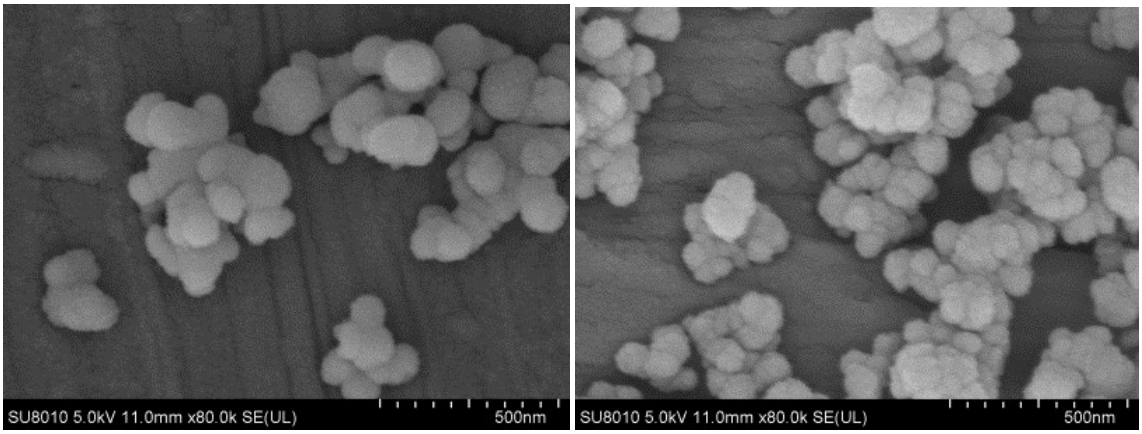

Fig. S17 SEM images of (a) IMSPF-Br-COOH+Fe^{3+}, and (b) IMSPF-Br-COOH+$Cr_2O_7^{2-}$. (IMSPF-Br-COOH was dispersed in ethanol, and then Fe^{3+} or $Cr_2O_7^{2-}$ was added. The mixture was stirred for 12 h and filtered to obtain IMSPF-Br-COOH+Fe^{3+} or IMSPF-Br-COOH+$Cr_2O_7^{2-}$).